A 220 GHz Code-Domain Focal Plane Imaging Radar with 0.78° Angular Resolution for Automotive Applications

Yinuo Xu, Arjang Hassibi, Thomas H. Lee
Department of Electrical Engineering, Stanford University, USA
yinuo@stanford.edu

***Abstract*— Next-generation advanced driver-assistance systems demand weather-robust millimeter wave imaging radars with high angular resolution. In this paper, we present a fully scalable, low-cost focal-plane imaging system with sub-degree angular resolution. The system employs a plastic Fresnel lens for beamforming, and an imaging array fabricated in 65 nm CMOS for 3D spatial information extraction. The prototype system operates at 220 GHz and achieves 0.78° angular resolution with 3 m range resolution.**

***Keywords*— millimeter wave, imaging, array processing**

I. Introduction

Advanced driver-assistance systems require high angular resolution sensors for object detection under varied weather conditions. Active millimeter wave (mm-wave) radars can achieve sub-degree angular resolution comparable to LiDAR, but are less affected by weather conditions such as rain and fog. For example, a sensor operating at 220 GHz can achieve 0.5° resolution with an aperture of 20 cm, with 15 dB less round-trip weather attenuation compared to LiDAR [1] [2].

Achieving high angular resolution at mm-wave frequency has been an active area of research. For automotive-specific applications, there are three major additional requirements: low cost, wide field-of-view (FoV), and high refresh rate.

Popular approaches, such as phased-arrays [3] and multiple-input multiple-output (MIMO) systems [4][5], reconstruct the angle of arrival (AoA) by employing phase shifters, at the cost of increased circuit complexity. The refresh rate of phased arrays is limited by the need to perform spatial scans to cover a wide FoV resulting from their narrow instantaneous spatial coverage. Digital AoA computation time similarly limits the refresh rate of MIMO systems. At narrow overall angular resolution and wide spatial coverage, refresh rate limitations lead to range measurement degradation due to object motion within a scan frame.

An alternative solution, which overcomes the aforementioned challenges and incurs no additional system latency, is to move the angle-extraction layer to free space by using a focal-plane structure, whose lens provides AoA extraction and whose array covers a wide instantaneous FoV [6]. In this paper, we demonstrate a simple, low-cost lens which provides passive AoA extraction. Further, unlike typical power- and area-hungry mm-wave receivers [3][4][5][7], we propose an envelope detection-based low cost, low latency, highly integrated and highly scalable sensor structure. This is achieved by leveraging the lens gain [8], using a coded on-off keying (OOK) waveform [7], and by exploiting rf-analog-digital co-design.

The rest of this paper is organized as follows: Section II provides an overview of the proposed system, Section III describes the lens and imaging array implementations, and Section IV presents measurement results.

II. System Overview

The proposed mm-wave imaging system, shown in Fig. 1, consists of a code-modulated mm-wave transmitter (TX), a plastic Fresnel lens, and an imaging receiver array. The proof-of-concept system uses an operating frequency of 220 GHz to provide an appropriate trade-off among wavelength, aperture size, cost, and attenuation in free space under varied weather conditions.

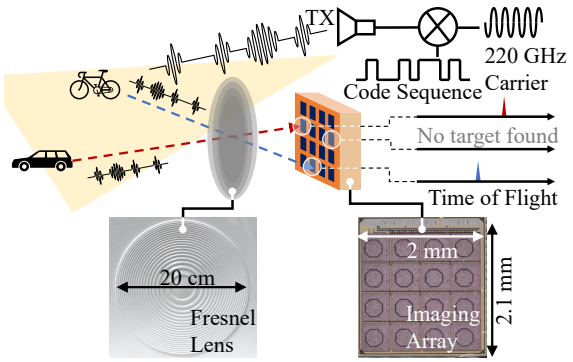

Fig. 1. Block diagram of the proposed focal plane imaging array. The prototype imaging array consists of a beamforming Fresnel lens and a 4×4 receiver array in 65 nm CMOS.

A coded OOK waveform is chosen for the following reasons: 1. Direct time-of-flight (ToF) extraction is simple to implement in digital systems which have easy clock accesses; 2. Unlike pulsed ToF sensors, which need high instantaneous TX power, coded OOK sensors require much less TX power, making a low-cost oscillator-based mm-wave TX suitable for such a system; 3. Orthogonal coding can be implemented for interference rejection, which is essential for large-scale automotive deployment.

During each measurement instance (subframe), the TX sends a coded pulse waveform. The reflections from the targets are focused by the lens onto the imaging array, where the pulses are detected continuously. As each pixel (unit receiver) receives reflected signals within a narrow solid angle defined by the lens, the target's angular information is extracted using

knowledge of the pixel location in the image plane. Finally, in-pixel matched filters identify the reflection and estimate the target's range using a ToF delay correlation (Fig. 2).

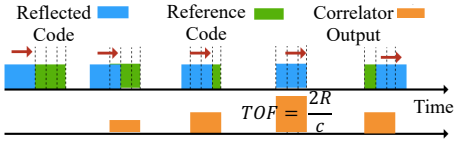

Fig. 2. ToF extraction from the code correlation delay.

The prototype lens is CNC machined and the 4×4-pixel imaging array is fabricated with a 65 nm CMOS process. Each pixel contains an on-chip antenna, an RF/mixed-signal front-end, and a code-correlation backend paired with in-pixel memory as shown in Fig. 4(a). As all sensing data is processed in real-time on chip, no extra computation latency is introduced. The total power consumption for 16 pixels is 19 mW: 9 mW for RF/mixed-signal and 10 mW for digital/memory at a 50 MHz clock frequency, enabling a practical design that can scale up to thousands of pixels to cover a still-wider FoV while meeting stringent cost, power, and latency requirements.

III. Implementation

A. Lens

The polyethylene (Dk = 2.1) Fresnel lens [8] is designed to be compatible with existing automotive injection-modeling processes. The lens is machined with a 0.9 mm engraving depth, and has a 20 cm diameter aperture, which translates to a 0.5° angular Rayleigh resolution.

B. Antenna and RF Front-End

The in-pixel front-end circuity, shown in Fig. 3, consists of a slot ring antenna, a Schottky diode [9] for envelope detection, and an amplifier-comparator chain for pulse reconstruction.

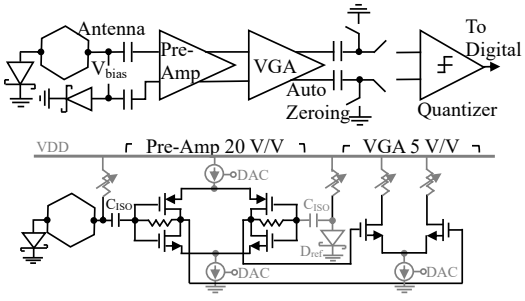

Fig. 3. Circuit diagram of analog front-end.

The proposed on-chip antenna is shown in Fig. 4(b). A ring slot architecture is chosen for its square footprint, which allows uniform spatial sampling and isolation between metal layers. The inner antenna metal allows diode biasing and provides the baseband signal path. The antenna is co-designed with the under-pixel circuits to maximize the radiation efficiency (25% at 220 GHz from simulation) and improve diode matching (simulated S11 of –16 dB).

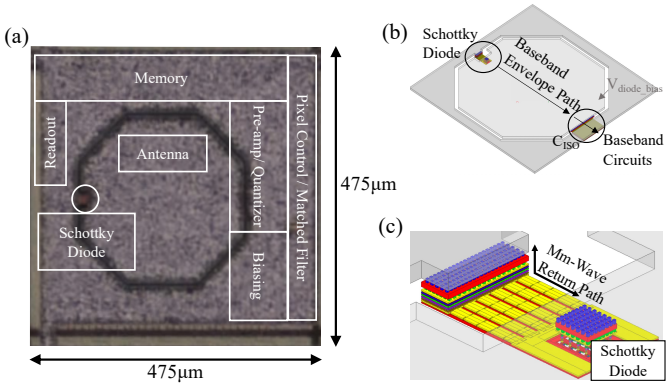

Fig. 4. (a) Chip micrograph, (b)(c) Antenna and Schottky diode design for baseband envelope path and mm-wave return path, respectively.

The front-end employs Schottky diodes because their cutoff frequency (measured to be 650 GHz when biased at its turn-on current of 60 µA) greatly exceeds that of the CMOS transistors in this process. Because each Schottky contact is as small as 90 nm square, sixteen Schottky contacts are grouped together as a single diode to reduce the effects of contact resistance variation. A 5 pF series MOM capacitor (C_{ISO}) connects the antenna and the baseband circuits which blocks the diode's DC biasing as well as 1/f noise.

As shown in Fig. 3, the downconverted envelope signal is amplified by a pseudo-differential voltage pre-amplifier, which is designed to reject the noise coupled from digital circuitry when paired with a biased reference diode. A variable gain amplifier (VGA) serves as a buffer to mitigate the injection of high-swing signals from the quantizer into the pre-amp. The gain of both amplifiers is controlled by an in-pixel R-2R DAC, and the amplifiers' offset is canceled through the use of auto-zeroing capacitors. The quantizer is a StrongARM comparator that reconstructs digital code sequences from the baseband envelope.

C. Back-End

The in-pixel back-end circuity consists of a code-based matched filter and a memory array, both with threshold control. Fig. 5 shows the design and timing diagram of the proposed back end. As the TX sends a 255-bit Gold-code sequence every subframe and the front-end reconstructs the received envelope, the quantizer digitizes the envelope and loads it into the matched filter at every clock cycle. The matched filter is made of an XNOR-based bitwise correlator which compares the incoming code and generates a moving sum of bit-level code that matches at different time instances. The time of flight is extracted from the self-correlation delay. A programmable 8-bit threshold control compares the correlation result and generates a 1 or 0 to indicate whether there is a target in the corresponding range bin. The result is then loaded into the memory array (accumulator) at the end of every subframe. The measurements are accumulated in the memory across subframes and read out at the end of each frame. At a code

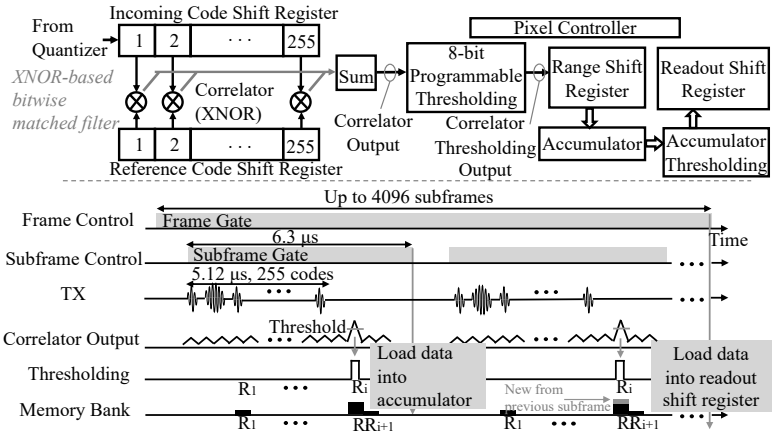

Fig. 5. Digital processor and timing diagram.

rate of 50 Mbit/s (corresponding to a 3 m range resolution), the memory provides a 25 ms per range-bin per pixel integration time.

The global controller manages readout, controls timing, and selects the pixels under test.

IV. Experimental Results

A. Lens Gain and Beam-Pattern Characterization

The Fresnel lens is characterized using a VDI SGX WR3.4 signal generation extender as the TX source, and an OML M05RF harmonic mixer with an R&S FSW spectrum analyzer as the receiver. Fig. 6(a) shows the received power with and without lens, indicating a 20 dB lens beamforming gain. The M05RF mixer is then mounted on a 2-axis linear stage for spatial scanning. The lens itself provides a measured 0.6° angular resolution at 219 GHz as shown in Fig. 6(b).

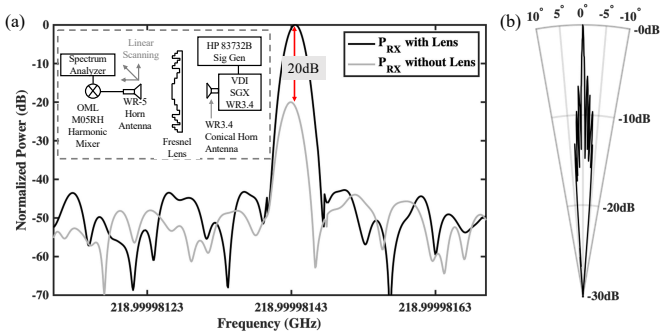

Fig. 6. Characterizations of (a) lens beamforming gain, and (b) lens beam pattern.

B. Imager Sensitivity and Beam-Pattern Characterization

To characterize the imager's sensitivity, two sets of frequency extenders and antennas are used to generate different free-space illumination powers: an R&S ZVA220 VNA extender (for low TX power) with a WR5 antenna, and a VDI SGX (for high TX power) with a WR3.4 antenna. An HP 8372B signal generator is paired with an Agilent 33250A arbitrary waveform generator to produce the modulated LO which drives the TX sets. The test chip is placed in the far field of the TX antennas and the illumination power is estimated using the Friis equation. All measurements are characterized at the correlator output with an integration time of 2.5 ms. The correlator SNR after post-processing is shown in Fig. 7(a). The estimated minimum detectable power per pixel is 1.15 nW per 2.5 ms integration time (for 0 dB SNR). Assuming a 15 dBm TX EIRP, this lens-receiver setup can detect objects (10 dB SNR) with a 4 m^2 radar cross-section at a range of 180 m with a 20 Hz refresh rate.

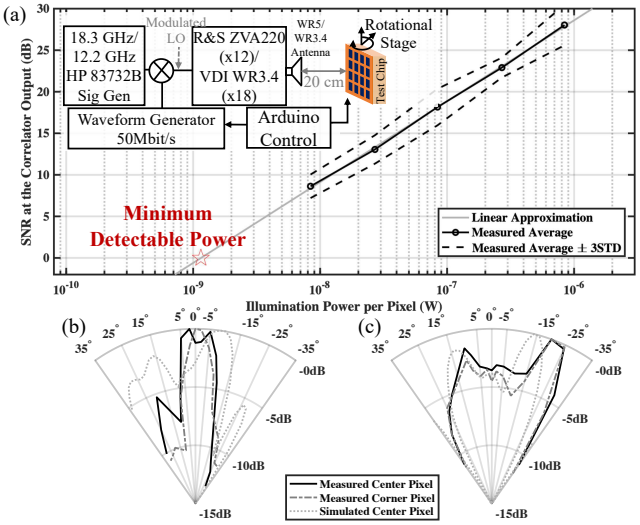

Fig. 7. (a) Characterization of receiver sensitivity with 2.5 ms integration time, (b) measurement, and (c) simulation of on-chip antenna H- and E-plane beam patterns.

For on-chip antenna beam pattern characterization, the test board is mounted on a rotation stage which is placed in the far field (20 cm) of the SGX WR3.4. The beam pattern is characterized by measuring the SNR at the correlator output at different angles. Fig. 7(b), (c) show the measured beam patterns at the center and the corner of the chip compared

with simulation results. The variation of antenna gain within a 10°×10° FoV is 3.6 dB.

C. System Characterization

Fig. 8 demonstrates the range measurement capability of the proposed system when a reflective target is placed 5 m away from the imaging system. The correlator readout matches the actual distance.

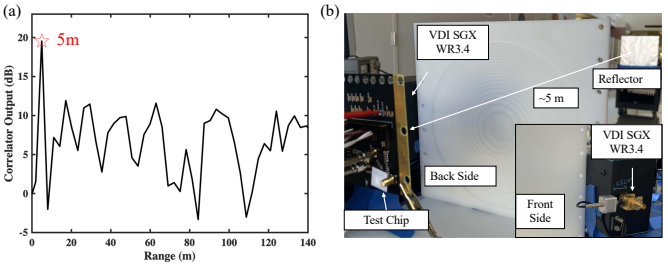

Fig. 8. Range measurement.

Fig. 9 shows the Airy disk image using the Fresnel lens and the prototype imaging array. The test imager is mounted on a 2-axis scanning stage to emulate a 1 cm × 1 cm (440 pixels) array at a distance of 22 cm (f1 focal plane) from the lens. The pulse-modulated TX source is placed 94 cm from the lens to generate a uniform plane wave. The diameter of the measured Airy disk on the focal plane is 3 mm, which maps to a 0.78° angular resolution for the full imaging system.

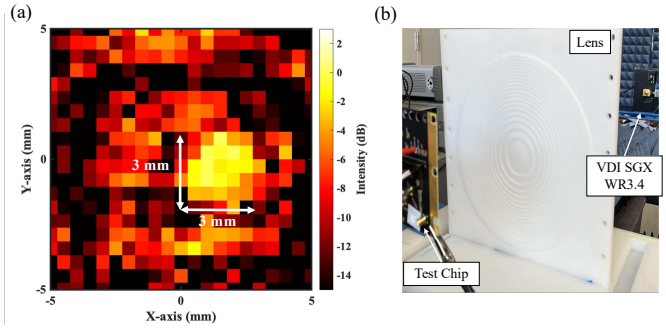

Fig. 9. Airy disk measurement for system angular resolution characterization.

Fig. 10 summarizes performance measurements and comparison with state-of-the-art radar mm-wave sensor chips. This array achieves the highest integration level, and smallest channel-area × power to wavelength^2 ratio. It is thus feasible to build a CMOS-based imaging array with hundreds of sensor which, when paired with a large-aperture lens, can achieve sub-degree resolution with more than 10°x10° instantaneous FoV coverage. Enabling low latency, high resolution, weather robust, low cost mm-wave automotive sensing.

V. Conclusion

In this paper, we present a 220 GHz coded OOK imaging system for weather-robust high-angular-resolution automotive sensing applications. The system adopts the plastic engraving lens design which provides a 20 dB passive beamforming gain with sub-degree beamwidth. A fully integrated scalable imager array with Schottky diode front-end, and pixel-level computation/memory is demonstrated. The whole system exhibits a measured angular resolution of 0.78° at 220 GHz.

	This Work	ISSCC'2019 [4]	ISSCC'2018 [5]	T THZ SCI TECHN'2020 [7]	JSSC'2019 [10]
Technology	65nm CMOS	28nm CMOS	45nm CMOS	65nm CMOS	65nm CMOS
Frequency (GHz)	220	77/79	77/79	183-205	240
Angular Res. (Degree)	0.78	1	-	-	16
Modulation Scheme	Coded OOK	GMSK-PMCW	FSK-FMCW	DS/SS	-
Scalability	Scalable on Chip	Scalable on Board	Scalable on Board	Scalable on Board	Scalable on Chip
Integration Level	Ant, RX, ADC, DSP, Mem	RX, ADC, DSP, Mem	RX, ADC, DSP	RX (w/ analog correlator)	Ant, RX
Power Per Channel (mW)	1.2	100[c]	292[c]	321	61.25
Area[a] per RX Element (mm^2)	0.226	1.87[b]	1.83[b]	1[b]	0.135
Area[a] x Power per RX Element /Wavelength^2	0.146	12.3	35	143	5.3

[a] Chip area only [b] Estimated from die photo [c] Virtual receiver

Fig. 10. Comparison table.

Acknowledgment

We gratefully acknowledge Ericsson, Keysight and Stanford SystemX for their generous funding support. We thank Prof. Amin Arbabian of Stanford, and Dr. Adrian Tang and Minji Zhu from UCLA for their kind equipment support. We also thank Dr. Jingzhi Zhang and Dr. Hao Nan for their valuable feedback in both design and testing.

References

[1] Z. Zhao et al., "Analytic Specific Attenuation Model for Rain for Use in Prediction Methods," *J. Infrared Millim. Terahertz Waves*, vol. 22, pp. 113-120, Jan. 2021.

[2] "Prediction methods required for the design of terrestrial free-space optical links", Rec. ITU-R P.1814, International Telecommunications Union, Aug. 2015.

[3] M. Li et al., "An Adaptive Analog Temperature-Healing Low-Power 17.7-to-19.2GHz RX Front-End with ±0.005dB/°C Gain Variation, <1.6dB NF Variation, and <2.2dB IP1dB Variation across -15 to 85°C for Phased-Array Receiver," *ISSCC*, pp. 230-232, 2011.

[4] V. Giannini et al., "A 192-Virtual-Receiver 77/79GHz GMSK Code-Domain MIMO Radar System-on-Chip," *ISSCC*, pp. 164-166, 2019.

[5] B. P. Ginsburg et al., "A multimode 76-to-81GHz automotive radar transceiver with autonomous monitoring," *ISSCC*, pp. 158-160, 2018.

[6] K. Button et al., *Infrared and Millimeter Waves V10: Millimeter Components and Techniques, Part II*, Cambridge (Mas.): Academic Press, 1983.

[7] A. Tang et al., "A Delay-Correlating Direct-Sequence Spread-Spectrum (DS/SS) Radar System-on-Chip Operating at 183–205 GHz in 28 nm CMOS," *IEEE Trans. Terahertz Sci. Technol.*, vol. 10, no. 2, pp. 212-220, Mar. 2020.

[8] D. Black et al., "Millimeter-wave characteristics of phase-correcting Fresnel zone plates." *IEEE Trans. Microw. Theory Techn.*, vol. 35, no.12, pp. 1122-1129, 1987.

[9] R. Han et al., "280-GHz Schottky Diode Detector in 130-nm Digital CMOS," *IEEE JSSC*, vol. 46, no. 11, pp. 2602-2612, Nov. 2011.

[10] Z. Hu et al., "A 32-Unit 240-GHz Heterodyne Receiver Array in 65-nm CMOS With Array-Wide Phase Locking," *IEEE JSSC*, vol. 54, no. 5, pp. 1216-1227, May 2019